Journal of Alloys and Compounds 506 (2010) 683–687

Contents lists available at ScienceDirect

Journal of Alloys and Compounds

journal homepage: www.elsevier.com/locate/jallcom

Synthesis and electrochemical properties of pure phase Zn_2SnO_4 and composite Zn_2SnO_4/C

W.S. Yuan, Y.W. Tian*, G.Q. Liu

School of Materials and Metallurgy, Northeastern University, Shenyang 110004, China

ARTICLE INFO

Article history:
Received 28 February 2010
Received in revised form 7 July 2010
Accepted 7 July 2010
Available online 15 July 2010

Keywords:
Zn_2SnO_4
Zn_2SnO_4/C
Lithium ion batteries
Anode
Electrochemical properties

ABSTRACT

Compound Zn_2SnO_4 was synthesized by a hydrothermal method in which $SnCl_4{\cdot}5H_2O$, $ZnCl_2$ and $N_2H_4{\cdot}H_2O$ were used as reactants. Composite Zn_2SnO_4/C was then synthesized through a carbothermic reduction process using the as-prepared Zn_2SnO_4 and glucose as reactants. The structure, morphology and electrochemical properties of the as-prepared products were investigated by means of X-ray diffraction, transmission electron microscopy and electrochemical measurements. The first discharge capacity of pure Zn_2SnO_4 was about 1634 mAh g^{-1}, with a capacity retain of 404.9 mAh g^{-1} in the 40th cycle at a constant current density of 60 mA g^{-1} in the voltage range of 0.05–3.0 V. Comparing to the pure Zn_2SnO_4, some improved electrochemical properties were obtained for composite Zn_2SnO_4/C. Its first discharge capacity was about 1436.8 mAh g^{-1}, with a capacity retain of 563.5 mAh g^{-1} in the 40th cycle.

1. Introduction

For lithium ion batteries, graphite is the most widely used material as anode so far. The theoretical capacity of graphite is about 372 mAh g^{-1} [1]. Once new material with higher capacity is developed, energy density of lithium ion batteries will be improved. Tin-based material exhibits higher capacity than graphite. For example, the theoretical capacity of SnO_2 can reach 1494 mAh g^{-1}, and its reversible theoretical capacity can also reach 781 mAh g^{-1}, having obvious advantage over graphite. Especially, various tin-based alloys, such as Cu–Sn [2,3], Al–Sn [4], Sn–Ni [5], Sn–Sb [6], Sn–Mo [7], etc., have been studying as a group of candidate materials for anode materials because their low cost and high energy densities. However, the poor capacity retention of these new materials during cycling as well as the large irreversible capacity during the first discharge/charge cycle has limited its commercial application [8–11]. Some improving measures are being considered to take, such as yielding nanomaterials with different shapes, and composite materials with carbon.

Recently, the reverse-spinel Zn_2SnO_4 attracts researchers' more attention since it has good electrochemical properties. For example, Rong et al. [12] synthesized the cube-shaped Zn_2SnO_4 by hydrothermal synthesis, and the anode revealed a reversible capacity of 580 mAh g^{-1} after the 50th cycles. Zhu et al. [13] synthesized reverse-spinel Zn_2SnO_4 by hydrothermal synthesis. Its first discharge and charge capacity were 1903.6 and 1045.5 mAh g^{-1}, respectively. But after 20 cycles, the capacity decayed rapidly to 644.7 mAh g^{-1}, with an average capacity fade rate of 3.3% per cycle. Hou et al. [14] synthesized inverse spinel structure Zn_2SnO_4 by a solid state reaction. Galvanostatic cycling showed 2054 mAh g^{-1} of initial discharge capacity and 1025 mAh g^{-1} of initial charge capacity. After 50 cycles, the specific charge capacity remained 689 mAh g^{-1} with a coulombic efficiency of approximately 98.8%, indicating excellent cycling stability and reversibility of this material. During the past few years, Zn_2SnO_4 has been successfully synthesized by various methods and showed good electrochemical properties. Nevertheless, the electrochemical features of Zn_2SnO_4/C composite have rarely reported.

In this study, a hydrothermal method is used to prepare pure Zn_2SnO_4, and then the as-prepared Zn_2SnO_4 react with glucose to produce composite Zn_2SnO_4/C. The carbon in composite can dissociate the metallic Sn and Zn particles and improve conductivity. So the electrochemical properties of composite Zn_2SnO_4/C can be improved.

2. Experimental

2.1. Synthesis procedures

At first, a hydrothermal method was employed to synthesize Zn_2SnO_4. In this process, analytical grade reagents $SnCl_4{\cdot}5H_2O$, $ZnCl_2$ and $N_2H_4{\cdot}H_2O$ were used as reactants. Tin chloride and zinc chloride were dissolved in distilled water to form transparent solutions under magnetic stirring. $N_2H_4{\cdot}H_2O$ was added dropwise into the mixture with the mole ratio of $ZnCl_2$:$SnCl_4$:$N_2H_4{\cdot}H_2O$ of 2:1:8. $N_2H_4{\cdot}H_2O$ immediately reacted with $ZnCl_2$ and $SnCl_4$ solutions and a slurry like white precipitate of the hybrid complex was formed. The final mixture was transferred into a

* Corresponding author.
E-mail address: yuanwansong2010@163.com (Y.W. Tian).

0925-8388/$ – see front matter © 2010 Elsevier B.V. All rights reserved.
doi:10.1016/j.jallcom.2010.07.042

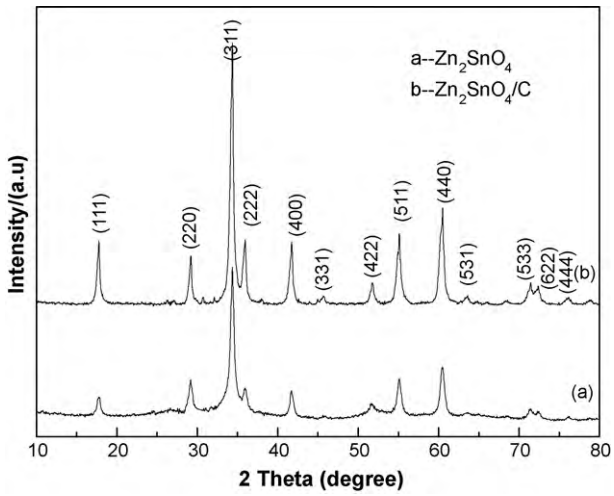

Fig. 1. XRD patterns of the as-prepared Zn_2SnO_4 and Zn_2SnO_4/C composite.

Teflon-lined stainless steel autoclave with a filling capacity of 80%. The autoclave was maintained at 180 °C for 24 h, and cooled naturally to room temperature. The solid products were concentrated and separated from the solvent by centrifugation, rinsed with distilled water and ethanol, and then dried at 80 °C for 12 h.

After pure Zn_2SnO_4 was obtained, the composite Zn_2SnO_4/C was then prepared through a carbothermic reduction process. The as-prepared Zn_2SnO_4 and glucose ($C_6H_{12}O_6$) were mixed together with a weight ratio of Zn_2SnO_4:$C_6H_{12}O_6$ = 85:15. This mixture was put into distilled water under magnetic stirring, and then dried at 80 °C. At last, the dried mixture was calcined at 600 °C for 2 h under Ar atmosphere to obtain composite Zn_2SnO_4/C.

2.2. Analysis of the active materials

The phase identification of the prepared samples was carried out by X-ray diffraction (XRD) using a Multiflex X-ray powder diffractometer (Rigaku Co. Ltd.). X-ray profiles were measured between 10° and 80° (2θ angle) with a monochromatic Cu Kα radiation source. Transmission electron microscopy (TEM, FEI Tecnai 12) was also employed to characterize the as-prepared samples.

2.3. Electrochemical test

The working electrode was prepared by mixing the active material, conducting carbon black, and binder (PVDF) at a weight ratio of 70/15/15. N-Methylpyrrolidone (NMP) was added as a solvent to form a homogeneous slurry. The slurry was cast uniformly on a copper foil. After dried at 120 °C for 12 h, a circular electrode with a diameter of 13 mm was punched from the copper foil and used as the working electrode with active material weight load of 4.52 mg/cm^2. Li foil as counter and reference electrodes. The electrolyte was 1 M $LiPF_6$ in a mixture of ethylene carbonate (EC)/diethyl carbonate (DMC)/ethylene methyl carbonate (EMC) (1:1:1 volume ratio). The cells were assembled in an argon-filled dry box. And charge–discharge tests were performed in the voltage range of 0.05–3.0 V at the current density of 60 mA g^{-1}. CV was conducted at a scan rate of 0.1 mV s^{-1} between 0.05 and 3.0 V versus Li/Li$^+$. Electrochemical impedance measurement was carried out by applying an ac voltage of 5 mV over the frequency range from 0.01 Hz to 100 kHz.

3. Results and discussion

Fig. 1 shows the XRD patterns of the as-prepared Zn_2SnO_4 and composite Zn_2SnO_4/C samples. It can be seen that all main diffraction peaks of the two samples are consistent with the (JCPDS, Card No. 24-1470) data of pure reverse spinel Zn_2SnO_4. The hydrothermal reaction mechanism can be described as follow:

$$SnCl_4 + 2ZnCl_2 + 8N_2H_4{\cdot}H_2O = Zn_2SnO_4 + 8N_2H_5Cl + 4H_2O \quad (1)$$

The appropriate conditions such as synthesized temperature, reaction time and stoichiometric proportion of reactants will make the above reaction take place completely. From the XRD patterns, the conditions taken in this study are appropriate. In addition, diffraction peaks intensity of composite Zn_2SnO_4/C is stronger than that of pure phase Zn_2SnO_4 because composite Zn_2SnO_4/C has been heat-treated at 600 °C.

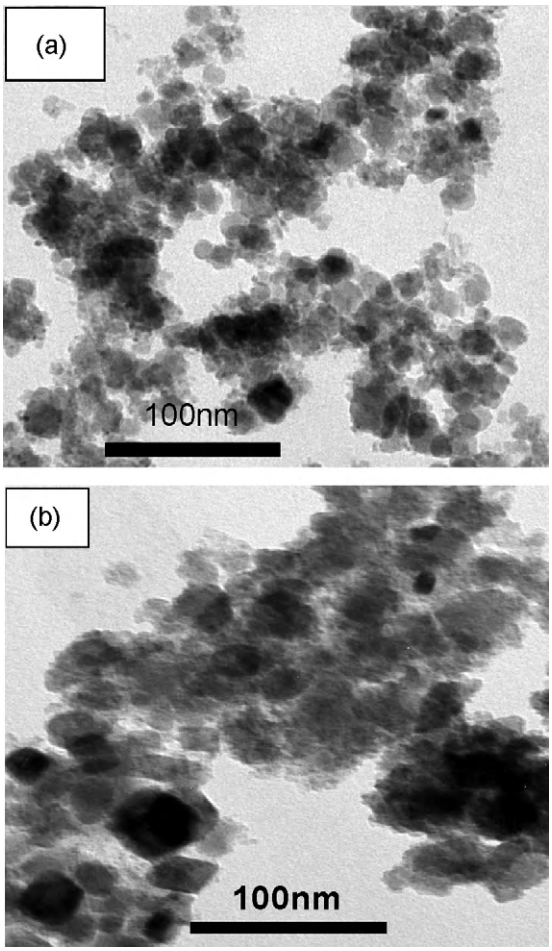

Fig. 2. TEM images of the product (a) as-prepared Zn_2SnO_4; (b) Zn_2SnO_4/C composite.

Fig. 2(a) and (b) displays TEM images of the as-prepared Zn_2SnO_4 and Zn_2SnO_4/C samples, respectively. It can be seen that Zn_2SnO_4 particles have irregular shapes and consisted of a number of small crystallites with a diameter between 20 and 30 nm. Composite Zn_2SnO_4/C particles also exhibit irregular shapes but the particle size is a bit larger.

The charge-discharge curves of Zn_2SnO_4 and Zn_2SnO_4/C samples are shown in Figs. 3 and 4, respectively. For pure phase Zn_2SnO_4, its first discharge capacity is about 1634 mAh g^{-1}, and first charge capacity is around 709.7 mAh g^{-1}. There is almost no capacity above the 1.0 V in the first discharge curve and a wide platform at around 1.0–0.5 V can be observed. The irreversible capacity in the first discharge is up to 924.3 mAh g^{-1}, which is different from the subsequent discharge. The reason is that the following reactions take place:

$$4Li^+ + Zn_2SnO_4 + 4e = Sn + 2Li_2O + 2ZnO \quad (2)$$

$$8Li^+ + Zn_2SnO_4 + 8e = 2Zn + Sn + 4Li_2O \quad (3)$$

$$xLi^+ + Sn + xe = Li_xSn\,(0 \le x \le 4.4) \quad (4)$$

$$yLi^+ + Zn + ye = Li_yZn\,(y \le 1) \quad (5)$$

The maximum amount of Li inserted into per mole Zn_2SnO_4 is 14.4 based on Eqs. (2)–(5), indicating the theoretical capacity of Zn_2SnO_4 is much larger than that of SnO_2. The large irreversible discharge capacity after the first cycle is probably due to severe side reaction with the electrolyte to form Li_2O and solid electrolyte interphase (SEI) film, especially for the nano-Zn_2SnO_4 particles with the small size and larger surface area. From the second cycle

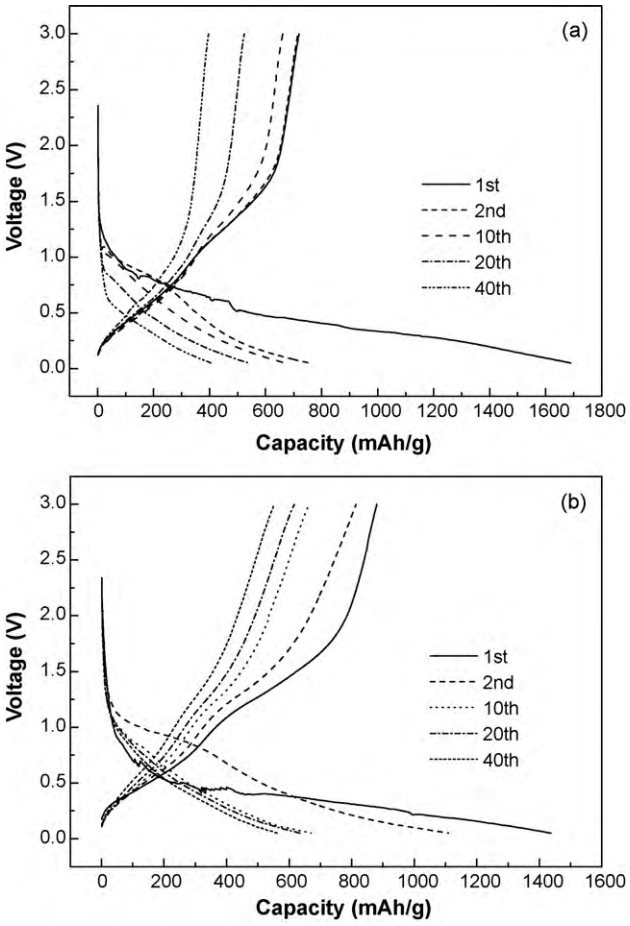

Fig. 3. Charge-discharge curves of product (a) as-prepared Zn_2SnO_4; (b) Zn_2SnO_4/C composite.

afterward, all the potential plateaus do not show a wide steady platform like the initial discharge, but display more inclined shape. The discharge platforms are different from the first discharge. Fig. 5 shows the XRD patterns of pure Zn_2SnO_4 electrode and Zn_2SnO_4 electrode after one charge-discharge cycle. It can be seen that the Zn_2SnO_4 particles are reduced to Zn and Sn in the discharge process. There is an obvious tendency for capacity to reduce. For example, the discharge capacities in the 20th and 40th cycle are 539.1 and 404.9 mAh g^{-1}, respectively. The reverse spinel structure of

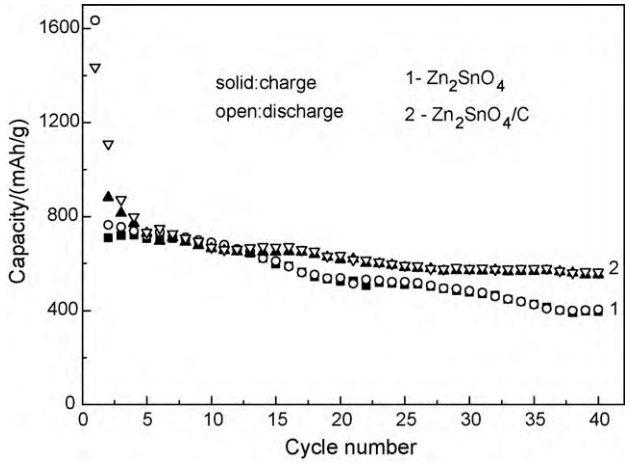

Fig. 4. Cycling performance of products.

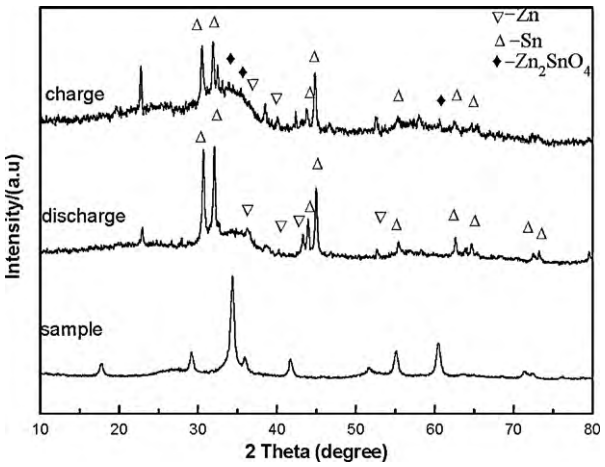

Fig. 5. XRD pattern of Zn_2SnO_4 electrode before and after the first charge–discharge.

Zn_2SnO_4 collapses when metallic Sn and Zn form, corresponding to Eqs. (2) and (3). The fine metallic Sn and Zn granular will aggregate. Lithium and Tin can form some alloys such as Li_2Sn_5, LiSn, Li_2Sn_5, Li_7Sn_3, Li_2Sn_5, Li_5Sn_2, $Li_{13}Sn_5$, Li_7Sn_2, $Li_{22}Sn_5$ [15], and lithium and

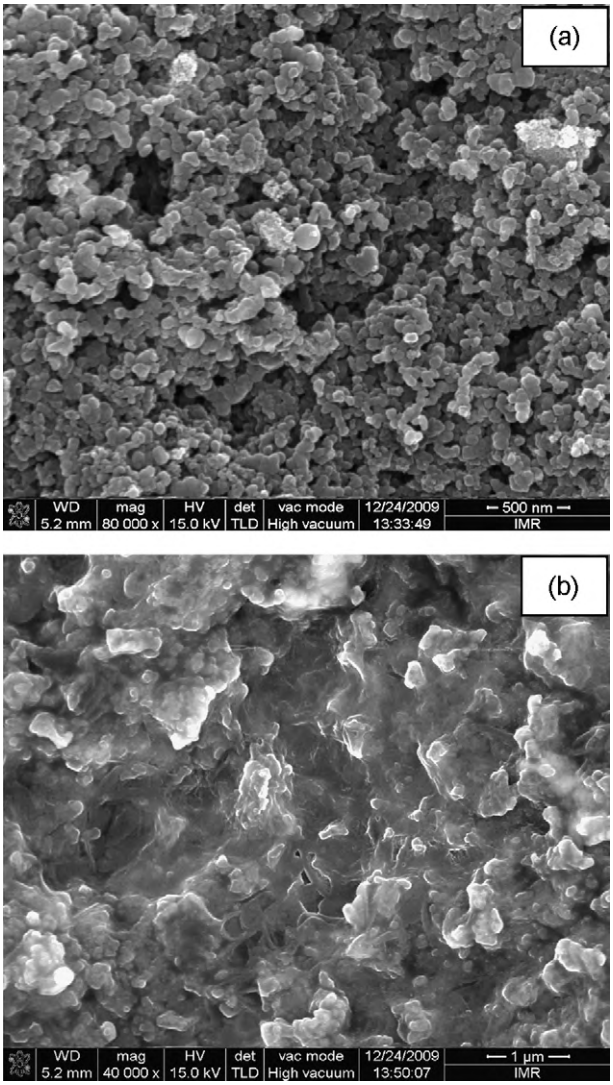

Fig. 6. SEM images of as-prepared Zn_2SnO_4 electrode. (a) Before cycle; (b) after the 40th cycle.

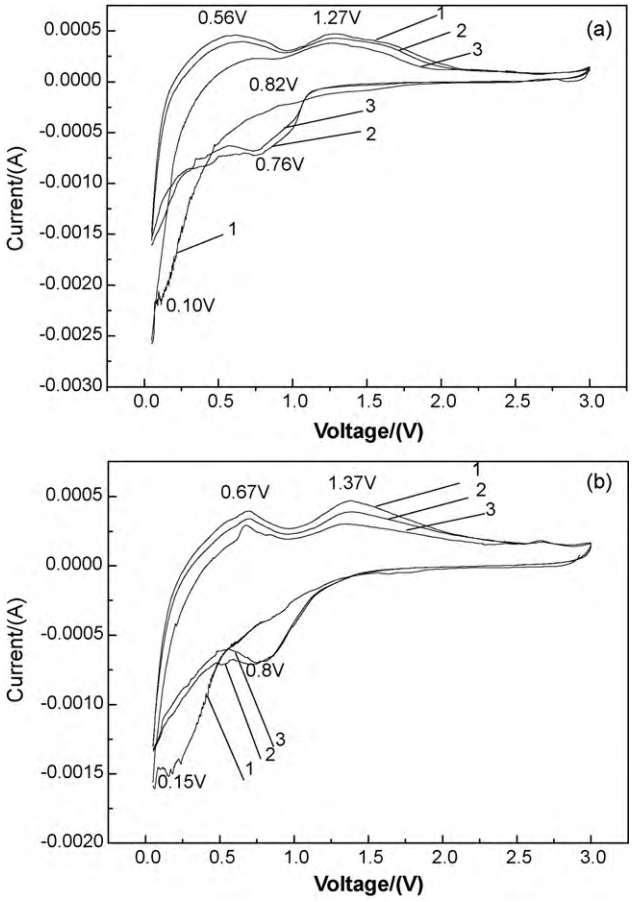

Fig. 7. Cyclic voltammograms of product at 1st, 2nd and 3rd cycles.

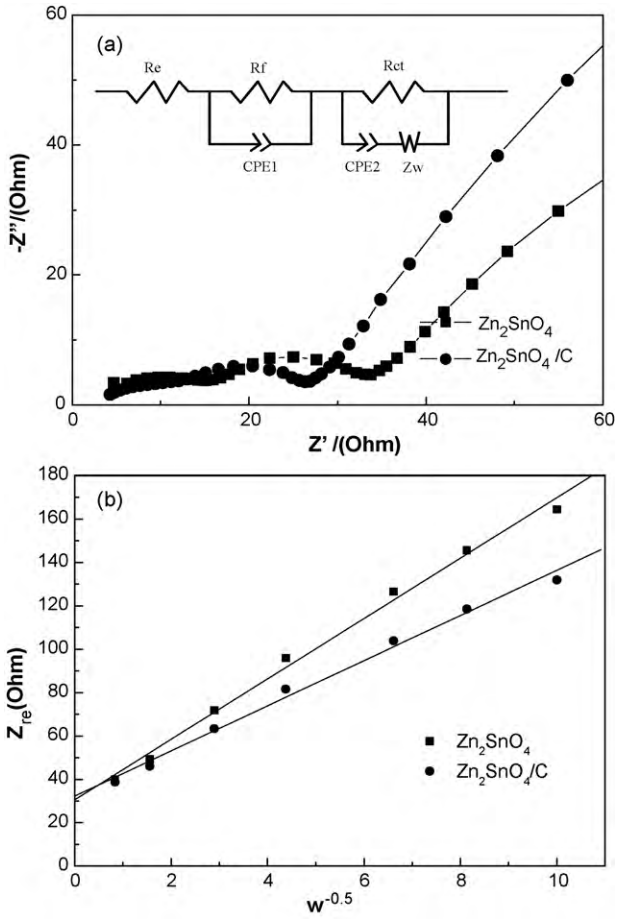

Fig. 8. (a) The Nyquist complex plane impedance plots of product after 40 cycles and the corresponding equivalent circuit and (b) the relationship between Z_{re} and $\omega^{-0.5}$ in the low frequency region.

zinc can form some alloys such as Li_2Zn_5, $LiZn_2$, Li_2Zn_3, LiZn [16]. So reaction equations (4) and (5) indicate that the amount of Li forming alloy with Sn and Zn are more than zero and less than 6.4. With these alloys forming, the volume will expand. For example, when Lithium and Tin form $Li_{22}Sn_5$, the volume will increase to 359% [17]. The SEM images of the Zn_2SnO_4 electrode and the one after the 40th cycle are shown in Fig. 6. It can be seen that pulverization and agglomeration occur between the active particles after 40th cycles, which will result in poor contact between the active particles and increase the electrode resistance. So the capacity decays rapidly.

For composite Zn_2SnO_4/C, its first discharge capacity is about 1436.8 mAh g^{-1}, and first charge capacity is around 880.5 mAh g^{-1}. The irreversible capacity is only 556.3 mAh g^{-1}. Compared with the pure Zn_2SnO_4, the Zn_2SnO_4/C composite has lower initial capacity. It exhibits better cycle ability than pure Zn_2SnO_4. In the 20th and 40th cycle, its capacities are 634.8 and 563.5 mAh g^{-1}, respectively. The better electrochemical properties of composite Zn_2SnO_4/C are ascribed to the carbon component. It can make metallic Sn or Zn granular separated from each other. So the volume expansion of Li–Sn and Li–Zn alloys can also be restrained during cycling. In addition, the carbon component also provides a highly conductive medium for electron transfer during the lithiation and de-lithiation process. So good electrochemical performance can be maintained.

The comparison of cycle ability between Zn_2SnO_4 and Zn_2SnO_4/C is shown in Fig. 4. The capacity retain rate of composite Zn_2SnO_4/C is obviously better than that of pure phase Zn_2SnO_4.

To further confirm the electrode change in structure, the XRD patterns of the pure Zn_2SnO_4 material and the Zn_2SnO_4 specimen taken from the electrode at the charged state and discharged state after one cycle is presented in Fig. 5. Three phases, inversed spinel Zn_2SnO_4, Zn and Sn, are detected at the charged state. It is found that most Li–Sn and Li–Zn alloy can be reversibly decomposed. In the case of the discharged state, the diffraction peaks of inversed spinel Zn_2SnO_4 disappear, but Zn and Sn exist. It proves that in the discharge process the Zn_2SnO_4 particles are reduced to Zn and Sn. And meanwhile, amorphous Li_2O as well as Li–Sn and Li–Zn alloy are also generated.

Cyclic voltammograms of product at 1st, 2nd and 3 rd cycles are shown in the Fig. 7. It can be seen from Fig. 7(a), the cathodic peak of pure Zn_2SnO_4 at first cycle is observed at 0.10 V, corresponding to multi-step electrochemical lithium reaction process and the first discharge curve. Meanwhile, two main anodic peaks are located at 1.27 and 0.56 V, corresponding to the delithiation process. In the second cycle, the cathode peaks shift to 0.76 V. The redox couple indexed as 0.76 V/1.27 V corresponds to the reversible reaction in Eqs. (2) and (3). In the following cycles, there is no substantial change for peak potentials and curve shape, which remains similar to those in the second cycle. There are some differences in cyclic voltammogram between pure Zn_2SnO_4 and composite Zn_2SnO_4/C. For composite Zn_2SnO_4/C, the redox couple corresponding to Eqs. (2) and (3) is at 0.80 V/1.37 V. Another oxidation peak appears at 0.67 V.

Fig. 8(a) shows the Nyquist complex plane impedance plots of product after 40 cycles and the corresponding equivalent circuit. It can be seen that they all comprise two semicircles in high and medium-frequency ranges as well as a line inclined at approximate 45° angle to the real axis in the low frequency

region. The AC impedance spectrum can be fitted by the equivalent circuit diagram. Re is the electrolyte resistance, and CPE1 and Rf are the constant phase element and resistance of the surface film and contact, respectively; CPE2 and Rct are the constant phase element and charge-transfer resistance, respectively; W is the Warburg impedance related to the diffusion of lithium ion into the bulk of composite electrodes. The charge-transfer resistance of pure Zn_2SnO_4 and composite Zn_2SnO_4/C were 16.88 and 11.52 Ω, respectively. The charge-transfer resistance of composite Zn_2SnO_4/C anode decreases significantly after 40th cycles in comparison with that of pure Zn_2SnO_4, which indicates a smaller electrochemical reaction resistance due to the carbon improved electronic contact between the active particles.

The diffusion coefficient of lithium ion can be calculated form the plots in the low-frequency region according to the following equation [18]:

$$D = \frac{R^2T^2}{2A^2n^4F^4C^2\sigma^2} \quad (6)$$

where R is the gas constant, T is the absolute temperature, n is the number of electron per molecule oxidized, A is the surface area, F is Faraday's constant, C is the concentration, D is the diffusion coefficient, and σ_w is the Warburg factor which has relationship with Z_{re} as follows:

$$Z_{re} = R_{ct} + R_e + \sigma_w\omega^{-0.5} \quad (7)$$

The relationship between Z_{re} and $\omega^{-0.5}$ in the low frequency region is shown in Fig. 8(b). The diffusion coefficient of lithium ion in the Zn_2SnO_4 and Zn_2SnO_4/C were calculated according to Eq. (6), were 1.40×10^{-12} and 1.74×10^{-10} cm^2 s^{-1}, respectively. It is clear that the diffusion coefficient of lithium ion was greatly increased by carbon adding, suggesting that carbon adding contributes to the enhancement of conductivity.

4. Conclusions

In summary, pure reverse spinel Zn_2SnO_4 and composite Zn_2SnO_4/C were synthesized by hydrothermal method and carbothermic reduction process. The composite Zn_2SnO_4/C showed a better electrochemical performance than pure phase Zn_2SnO_4, with a much higher capacity (563.5 mAh g^{-1}) after 40 cycles. The carbon component could buffer the volume expansion of Li–Sn and Li–Zn alloys and provided a highly conductive medium for electron transfer, improving the cycle capability of anode material Zn_2SnO_4.

References

[1] Y.P. Wu, C. Jiang, C. Wu, R. Holze, Solid State Ionics 156 (2003) 283–290.
[2] S. Liu, Q. Li, Y.X. Chen, F.J. Zhang, J. Alloys Compd. 478 (2009) 694–698.
[3] F.S. Ke, L.S. Cai, S.G. Sun, Electrochim. Acta 52 (2007) 6741–6747.
[4] R.Z. Hu, M.Q. Zeng, C.Y.V. Li, M. Zhu, J. Power Sources 188 (2009) 268–273.
[5] J. Hassoun, S. Panero, P. Simon, P.L. Taberna, B. Scrosati, Adv. Mater. 19 (2007) 1632.
[6] Z. Wang, W.H. Tian, X.G. Li, J. Alloys Compd. 439 (2007) 350–354.
[7] Y. Liang, Z.G. Tian, H.J. Liu, R. Peng, J. Alloys Compd. (2010), doi:10.1016/j.jallcom.2010.05.082.
[8] T. Moon, C. Kim, S.T. Hwang, B. Park, Electrochem. Solid-State Lett. 9 (2006) A408–A411.
[9] J.Y. Lee, R.F. Zhang, Z.L. Liu, J. Power Sources 90 (2000) 70–75.
[10] G.X. Wang, Y. Chen, L. Yang, J. Yao, S. Needham, H.K. Liu, J.H. Ahn, J. Power Sources 146 (2005) 487–491.
[11] S. Machill, T. Shodai, Y. Sakurai, J. Yamaki, J. Power Sources 73 (1998) 216–223.
[12] A. Rong, X.P. Gao, G.R. Li, T.Y. Yan, H.Y. Zhu, J.Q. Qu, D.Y. Song, J. Phys. Chem. B 110 (2006) 14754–14760.
[13] X.J. Zhu, L.M. Geng, F.Q. Zhang, Y.X. Liu, L.B. Cheng, J. Power Sources 189 (1) (2009) 828–831.
[14] X.H. Hou, Q. Cheng, Y. Bai, W.F. Zhang, Solid State Ionics 181 (2010) 631–634.
[15] Y. Idota, T. Kubota, A. Matssufuji, Y. Maekawa, T. Mi-yasaka, Science 276 (1997) 1395–1397.
[16] F. Belliard, J.T.S. Irvine, J. Power Sources 97 (2001) 219–222.
[17] I.A. Courtney, J.R. Dahn, J. Electrochem. Soc. 144 (6) (1997) 2043–2052.
[18] Q. Cao, H.P. Zhang, G.J. Wang, Q. Xia, Y.P. Wu, H.Q. Wu, Electrochem. Commun. 9 (2007) 1228–1232.